Studies on a Nonequilibrium Continuum Traffic Flow Model with Frozen "Sound Wave" Speed

November 15, 2002

W.L. Jin

Department of Mathematics

University of California

Davis, CA 95616

Tel: 530-752-0828

Fax: 530-752-6635

E-mail: wjin@ucdavis.edu

H.M. Zhang

Department of Civil and Environmental Engineering

University of California

Davis, CA 95616

Tel: 530-754-9203

Fax: 530-752-7872

E-mail: hmzhang@ucdavis.edu

Word Count: 7500 (approximately)

ABSTRACT

In this paper, we present some results from a recent study on a variation of a new nonequilibrium continuum traffic flow model, where "traffic sound speed" is constant. (We hence call this model "frozen-wave" model.) This model resembles the Payne-Whitham model but avoids "back-traveling" of the latter. For this "frozen-wave" model, we analyze the Riemann problem for its homogeneous system, develop two numerical solution methods to solve it, and carry out numerical simulations under both stable and unstable traffic conditions. These results show that, under stable conditions, the model behaves similarly to the Payne-Whitham model. However, under unstable traffic conditions, it has non-physical solutions or no solutions when a "vacuum problem" occurs. This study, on one hand, provides a more complete picture of the properties of this "frozen-wave" model and reduces the risk of improper applications of this model. On the other hand, it also highlights the need to adopt a density-dependent sound speed.

1 INTRODUCTION

More and more traffic congestions in metropolitan cities during peak hours have made it a major task for traffic engineers to tackle the traffic congestion problem. As the basis of this mission, a good understanding of traffic phenomena is generally achieved by establishing models of traffic dynamics. Among the many existing traffic models, continuum traffic flow models, which can be expressed and analyzed clearly with well-developed mathematical tools and are efficient for numerical simulations, have been widely applied in the study of traffic phenomena and in the development of intelligent transportation management strategies.

In continuum traffic flow models, the movements of vehicles are studied collectively through combinations of basic waves such as decelerating (shock) waves and accelerating (rarefaction) waves. In these models, traffic conditions at location x and time t are described by three aggregate quantities: traffic density $\rho(x,t)$, space-mean speed $v(x,t)$, and flow rate $q(x,t)(=\rho v)$. Observations of traffic suggest that there is a fundamental relationship between ρ and q (or v). For example, when traffic is more congested; i.e., when ρ is bigger, vehicles generally travel at a lower speed. This means v is non-increasing in ρ. Also, $q = 0$ when $\rho = 0$ or ρ_j (the jam density when traffic is bumper to bumper), and q attains its maximum (the capacity) for a critical density. Thus, it is assumed that, when traffic is in "equilibrium"[1], there exists a fundamental diagram: $q = Q(\rho)$; i.e., in equilibrium traffic, flow rate is uniquely determined by traffic density. Consequently, we have an equilibrium relationship between ρ and v: $v = V(\rho) \equiv Q(\rho)/\rho$.

Moreover, during a time period, the increment in the number of vehicles on a road section is equal to the difference between the in-flow and out-flow. This fact

[1]Here equilibrium means $q(x,t)$, $\rho(x,t)$, and $v(x,t)$ do not change over time t.

leads to the following traffic conservation equation:

$$\rho_t + q_x = 0. \tag{1}$$

Equation 1 together with the assumption that traffic is in equilibrium gives us the celebrated LWR (Lighthill-Whitham-Richards) model (1, 2):

$$\rho_t + (\rho V(\rho))_x = 0. \tag{2}$$

Although the LWR model is capable of simulating shock and rarefaction waves in traffic, it fails to capture other interesting phenomena exhibited in realistic traffic. For example, in real traffic, flow rate generally does not follow the change of traffic density in a unique manner. Besides, the LWR model can not explain the instability in traffic flow, such as the formation of vehicle clusters from initially homogeneous traffic conditions. Therefore, there is a need to develop nonequilibrium models that could overcome these drawbacks of the LWR model.

The first nonequilibrium continuum model, the Payne-Whitham (PW) model, was developed in (3, 4). In this higher-order model, one more equation is introduced besides Equation 1 to capture the change of velocity in a similar way of modeling momentum dynamics in fluid flow:

$$v_t + vv_x + \frac{c_0^2}{\rho}\rho_x = \frac{V(\rho) - v}{\tau}, \tag{3}$$

where c_0 is the so-called traffic sound speed, and τ the relaxation time. In (5, 6), it was shown that the PW model can simulate stable traffic like the LWR model and, in addition, is capable of modeling the formation of vehicle clusters. However, the PW model has drawn some criticism since it allows wave solutions with speed higher than vehicle travel speed and may cause back-traveling (or negative-speed) (7).

In order to avoid the drawbacks of the PW model, Aw and Rascle (8) proposed

the following model based on a mathematical argument:

$$\begin{aligned} \rho_t + (\rho v)_x &= 0, \\ v_t + (v - \rho p'(\rho))v_x &= \tfrac{V(\rho)-v}{\tau}, \end{aligned} \tag{4}$$

where $p(\rho)$ is a pressure law. However, how $p(\rho)$ is related to driver-behavior was not specified in their study. So this model can be considered as a general framework of a class of nonequilibrium models.

Following the same approach in developing a PW-like model (9),

$$\begin{aligned} \rho_t + (\rho v)_x &= 0, \\ v_t + v v_x + \tfrac{(\rho V'(\rho))^2}{\rho}\rho_x &= \tfrac{V(\rho)-v}{\tau}, \end{aligned} \tag{5}$$

Zhang (10) derived a model similar to Aw and Rascle's model from a car-following model:

$$\begin{aligned} \rho_t + (\rho v)_x &= 0, \\ v_t + (v + \rho V'(\rho))v_x &= \tfrac{V(\rho)-v}{\tau}, \end{aligned} \tag{6}$$

which provides a physical explanation to $p(\rho)$ $(= -V(\rho))$. For the purpose of exposition, we will refer to this model as the ARZ (Aw-Rascle-Zhang) model. The ARZ model no longer admits wave solutions faster than traffic and avoids back-traveling (8, 10). However, this model is always stable (11) and, therefore, loses PW model's ability of simulating unstable traffic and vehicle clusters[2].

Interestingly, another similar model was proposed in (13) as

$$\begin{aligned} \rho_t + (\rho v)_x &= 0, \\ v_t + (v - c_0)v_x &= \tfrac{V(\rho)-v}{\tau}, \end{aligned} \tag{7}$$

which is also in the framework of Equation 4, with the pressure function $p = c_0 \ln \rho$. Here c_0 is the speed of 1-waves (see sections 2 and 3 for explanations of 1-waves)

[2]Instability can be introduced to the ARZ model by considering time delays in the underlying car-following model, which lead to $p(\rho) = -\gamma V(\rho)$ (12).

relative to moving traffic. Analogous to sound propagation in physical medium, we call c_0 traffic sound speed. In general, sound wave speed c is dependent on traffic conditions, i.e. $c = c(\rho)$. We can consider c_0 in Equation 7 as being frozen at a particular ρ_0, i.e. $c_0 = c(\rho_0)$. Hence we shall refer Equation 7 as the frozen-wave model to highlight this fact. The frozen-wave model also removes the drawbacks of the PW model according to (8, 10). All three models, Equation 4, Equation 6, and Equation 7, eliminates the "back-traveling" and faster-than-traffic waves found in the PW model and hence are anisotropic. Because the sound speed in Equation 7 is constant as in the PW model, this model most resembles the PW model and appears to be an ideal alternative of the PW model.

In this paper, we present some recent studies on the frozen-wave model given by Equation 7. The studies include the analysis of the Riemann problem for the homogeneous model (i.e. Equation 7 without relaxation), the development of two numerical methods: the Godunov method (14) (based on solutions of the Riemann problem) and the fifth order Weighted Essentially Non-Oscillatory (WENO) (15) method (requiring no Riemann solvers as in Godunov), and numerical simulations using the two methods. These studies show that, under stable traffic conditions, the frozen-wave model behaves similarly to the PW and LWR models. However, under certain initial conditions, the Riemann problem of the frozen-wave model is ill-posed and its solutions are no longer physical (traffic densities can exceed the jam density or there are no solutions). Furthermore, numerical simulations reveal that non-physical solutions occur when the model is unstable.

The rest of this paper is organized as follows. First, we study the frozen-wave model as a hyperbolic system of conservation laws with relaxation (Section 2). In Section 3, the Riemann problem of the homogeneous frozen-wave model is discussed. In this Section, we also present the Godunov method for this model. In Section 4,

we present the fifth order WENO method for this model. In Section 5, we apply the two numerical methods to simulate both stable and unstable traffic and compare the results with those of the PW and LWR models. Finally, we draw some conclusions in Section 6.

2 THE FROZEN-WAVE MODEL AS A HYPERBOLIC SYSTEM OF CONSERVATION LAWS WITH RELAXATION

The frozen-wave model can be rewritten as

$$u_t + f(u)_x = s(u), \tag{8}$$

where

$$u = \begin{bmatrix} \rho \\ v \end{bmatrix}, \qquad f(u) = \begin{bmatrix} \rho v \\ \frac{1}{2}v^2 - c_0 v \end{bmatrix} \qquad s(u) = \begin{bmatrix} 0 \\ \frac{V(\rho)-v}{\tau} \end{bmatrix}. \tag{9}$$

Hence the model becomes a hyperbolic system of conservation laws with relaxation in the sense of (16, 4, 17). For such a system, we are generally interested in the properties of its homogeneous version and its stability.

2.1 The Homogeneous Model

The homogeneous model of Equation 7,

$$\begin{bmatrix} \rho \\ v \end{bmatrix}_t + \begin{bmatrix} \rho v \\ \frac{1}{2}v^2 - c_0 v \end{bmatrix}_x = 0, \tag{10}$$

is in a *conservative form*, $u_t + f(u)_x = 0$, where the Jacobian matrix of the flux function $f(u)$ is

$$\partial f \;=\; \begin{bmatrix} v & \rho \\ 0 & v - c_0 \end{bmatrix},$$

whose eigenvalues are $\lambda_1 = v - c_0$ and $\lambda_2 = v$. The right and left eigenvectors corresponding to $\lambda_{1,2}$ are respectively

$$r_1 = \begin{bmatrix} -\rho/c_0 \\ 1 \end{bmatrix}, \qquad l_1 = \begin{bmatrix} 0 & 1 \end{bmatrix};$$

$$r_2 = \begin{bmatrix} 1 \\ 0 \end{bmatrix}, \qquad l_2 = \begin{bmatrix} 1 & \rho/c_0 \end{bmatrix}.$$

The relationships between the eigenvalues and eigenvectors are $l_1 \cdot r_1 = 1$, $l_2 \cdot r_2 = 1$, $l_1 \cdot r_2 = 0$, $l_2 \cdot r_1 = 0$, and

$$L \cdot \partial f \cdot R = \Lambda,$$

where

$$L = \begin{bmatrix} l_1 \\ l_2 \end{bmatrix}, \qquad R = \begin{bmatrix} r_1 & r_2 \end{bmatrix}, \qquad \Lambda = \begin{bmatrix} \lambda_1 & 0 \\ 0 & \lambda_2 \end{bmatrix}.$$

Note that the left and right transformation matrix L and R are functions of u, and they can be written as $L(u)$ and $R(u)$.

Let $w = L \cdot u$, we then have the locally diagonalized version of the homogeneous model,

$$w_t + \Lambda w_x \;=\; 0. \tag{11}$$

In Equation 8, the eigenvalues of the Jacobian matrix, $\lambda_{1,2}$, which are also known as characteristic speeds, determine the propagation speed of a small perturbation in

traffic. Since $\lambda_{1,2} \leq v$, no waves in this model can travel faster than traffic itself. Moreover, it has been shown that back traveling phenomena do not appear in this model (8, 10, 13).

2.2 Stability Properties of the Frozen-Wave Model

As a hyperbolic system of conservation laws with relaxation, Equation 8 has the LWR model, Equation 2, as its subsystem. I.e., when τ goes to 0, Equation 8 admits the same stable solutions as Equation 2. Note that the LWR model has the eigenvalue $\lambda_* = V(\rho) + \rho V'(\rho)$.

Whitham (4) showed that the stability condition for the linearized system of a system like Equation 8 is

$$\lambda_1 < \lambda_* < \lambda_2. \tag{12}$$

Liu (17) showed that if Equation 12 is always satisfied, then the corresponding frozen-wave model is stable under small perturbations and its time-asymptotic solutions are completely determined by the equilibrium LWR model. Chen et al. (18) showed that if inequalities 12 are satisfied, then solutions of the frozen-wave model tend to the solutions of the LWR model as the relaxation time tends to zero. In (13), it is asserted that Equation 12 is the stability condition for Equation 7. Therefore, if Equation 12 is violated, solutions are not stable and very sensitive to small changes in initial conditions.

As it is always true that $\lambda_* \leq \lambda_2$ in Equation 7, the stability condition is only violated when $\lambda_1 > \lambda_*$. In this paper, we will show the numerical simulations of the frozen-wave model under both stable and unstable initial traffic conditions.

3 THE RIEMANN PROBLEM OF THE HOMOGENEOUS MODEL AND THE GODUNOV NUMERICAL SOLUTION METHOD

In this section, we first analyze the Riemann problem of the homogeneous system, Equation 10, and, based on this, develop the Godunov method for solving Equation 7, the frozen-wave model.

3.1 Wave Solutions of the Riemann Problem for the Homogeneous System

We consider the Riemann problem for the homogeneous version of Equation 7 with the following jump initial condition

$$u = \begin{cases} u_l, & x < 0; \\ u_r, & x > 0. \end{cases}$$

According to (19), the Riemann problem is solved by a combination of two families of waves: 1-waves corresponding to λ_1 and 2-waves corresponding to λ_2. Since

$$\nabla\lambda_1 \cdot r_1 = -\frac{c_0}{\rho} \neq 0, \qquad \nabla\lambda_2 \cdot r_2 = 0,$$

1-waves are genuinely nonlinear and 2-waves are linearly degenerate (8, 10).

In the following part, we find the curves in (ρ, v)-plane for basic 1-waves and 2-waves of the Riemann problem with (u_l, u_r).

1. Shock waves. Corresponding to λ_1 and λ_2, the Riemann problem may have 1-shock wave solutions and 2-shock wave solutions as follows.

(a) 1-shock waves. From (20), the 1-shock waves satisfy

$$\lambda_1(u_r) < s < \lambda_1(u_l), \qquad s < \lambda_2(u_r), \tag{13}$$

where the shock wave speed s is given as follows,

$$s \;=\; \frac{[\rho v]}{[\rho]} = \frac{[\frac{1}{2}v^2 - c_0 v]}{[v]}. \tag{14}$$

Here $[\cdot] = (\cdot)_l - (\cdot)_r$.

From the above equations and conditions, we find the 1-shock wave curve

$$\mathbf{S_1}: \qquad v - v_l = -2c_0\frac{\rho - \rho_l}{\rho + \rho_l}, \qquad \rho > \rho_l, v < v_l. \tag{15}$$

(b) 2-shock waves. The 2-shock waves satisfy the following conditions

$$\lambda_2(u_r) < s < \lambda_2(u_l), \qquad s > \lambda_1(u_l). \tag{16}$$

Therefore 2-shock waves satisfy

$$\mathbf{S_2}: \qquad v = v_l, \qquad \rho > \rho_l. \tag{17}$$

2. Rarefaction waves. Similarly, corresponding to the two eigenvalues, there are two types of rarefaction waves: 1-rarefaction waves and 2-rarefaction waves.

(a) 1-rarefaction waves. The 1-rarefaction waves satisfy $(\partial f(u) - \lambda_1(u))u_\xi = 0$, thus we have

$$\mathbf{R_1}: \qquad v - v_l = -c_0 \ln\frac{\rho}{\rho_l}, \qquad \rho < \rho_l, v > v_l. \tag{18}$$

(b) 2-rarefaction waves. Similarly, we obtain the 2-rarefaction waves in the (ρ, v)-plane as

$$\mathbf{R_2}: \qquad v = v_l, \qquad \rho < \rho_l. \tag{19}$$

The Riemann invariants for the two rarefaction wave solutions can be written as follows

$$\mathbf{RI_1}: \qquad w = v + c_0 \ln \rho, \tag{20}$$

$$\mathbf{RI_2}: \qquad w = v. \tag{21}$$

From the above analysis, we can see that 2-waves, including 2-shock and 2-rarefaction waves, are in fact contact waves[3]. Hereafter, we denote 2-waves by C (contact waves), S_2 by CS (contact shock), and R_2 by CR (contact rarefaction).

In Figure 1, 1-rarefaction, 1-shock, and contact waves starting from u_l are depicted in the (ρ, v)-plane. These curves divide the (ρ, v)-plane into four regions. From (19), when u_r is in one of these regions, the Riemann problem with (u_l, u_r) is solved by a combination of two basic waves. Namely, we may have the following solutions: 1-shock wave (S_1) when u_r is on the S_1 branch; 1-rarefaction wave (R_1) when u_r is on the R_1 branch; contact wave, including CS and CR waves, when $v_r = v_l$; 1-shock+contact wave when $v_r < v_l$; 1-rarefaction+contact wave when $v_r > v_l$. For the solutions combining two waves, we can define an intermediate state u_m so that the Riemann problem with (u_l, u_m) is solved by a 1-wave and the Riemann problem with (u_m, u_r) is solved by a contact wave.

3.2 Solutions of u at $x = 0$

In this subsection, we discuss the solution of u from the Riemann problem of Equation 10 with (u_l, u_r) at $x = 0$, denoted by u_0^*, and present the formulas for computing u_0^* for the cases when the Riemann problem is solved by the two types of waves: $R_1 - C$, which is a combination of a 1-rarefaction wave and a contact wave, and $S_1 - C$, which

[3]Contact waves interface two traffic states that have the same velocity but different densities.

is a combination of 1-shock and a contact wave. Note that the situations when the solutions of only a 1-wave or a contact wave can be considered as their special cases.

1. When we have $R_1 - C$ solutions, the intermediate state satisfies

$$\begin{aligned} v_m - v_l &= -c_0 \ln \frac{\rho_m}{\rho_l}, \\ v_m - v_r &= 0. \end{aligned}$$

From them, we obtain the intermediate state (ρ_m, v_m),

$$v_m = v_r, \tag{22}$$

$$\rho_m = \rho_l e^{-\frac{v_r - v_l}{c_0}} < \rho_l. \tag{23}$$

Then we can obtain the boundary values u_0^* as follows:

(a) When $\lambda_1(u_m) = v_m - c_0 < 0$, we have $u_0^* = u_m$;

(b) When $\lambda_1(u_l) > 0$, we have $u_0^* = u_l$;

(c) When $\lambda_1(u_l) < 0 < \lambda_1(u_m)$, we have $v_0^* = c_0$ and $\rho_0^* = \rho_l e^{-\frac{c_0 - v_l}{c_0}}$.

2. When we have $S_1 - C$ solutions, the intermediate state satisfies

$$\begin{aligned} v_m - v_l &= -2c_0 \frac{\rho_m - \rho_l}{\rho_m + \rho_l}, \\ v_m - v_r &= 0. \end{aligned}$$

Note that $v_m > v_l - 2c_0$ for all $\rho_m > 0$. Thus, there is no solution when $v_r \leq v_l - 2c_0$. In this case, a "vacuum problem" occurs (19). When $v_r > v_l - 2c_0$, we have the intermediate state $(v_m = v_r)$

$$\rho_m = \rho_l \frac{2c_0 - v_r + v_l}{2c_0 + v_r - v_l}. \tag{24}$$

Defining shock wave speed

$$s = \frac{\rho_m v_m - \rho_l v_l}{\rho_m - \rho_l},$$

we have the following results: when $s \geq 0$, $u_0^* = u_l$; otherwise, we have $u_0^* = u_m$.

However, in Equation 24, when

$$v_r < v_l - 2c_0\frac{\rho_j - \rho_l}{\rho_j + \rho_l}, \tag{25}$$

we will obtain non-physical intermediate traffic density $\rho_m > \rho_j$ or have no solution at all (the condition that $v_r \leq v_l - 2c_0$ is contained in condition 25). Therefore, when condition 25 is satisfied, the frozen-wave model has non-physical solutions or no solutions when a vacuum problem occurs. This property, which has not been shown before, determines that this model has significant limitations. By numerical simulations, we will show that condition 25 is satisfied when traffic is unstable.

3.3 The Godunov Method

In the previous subsection, we present the formulas for computing u at a jump point. Based on this, here we are able to develop the Godunov method (14) for solving the frozen-wave model given by Equation 7.

To apply the Godunov method, we partition our road of interest $[0, L]$ into N cells with length $\Delta x = L/N$ and discretize the time interval $[0, T_0]$ into K time steps with length $\Delta t = T_0/K$. Then Equation 8 can be approximated by the following Godunov-type finite difference equation,

$$U_i^{j+1} = U_i^j - \frac{\Delta x}{\Delta t}(f(U_{i+1/2}^{*j}) - f(U_{i-1/2}^{*j})) + \Delta t\tilde{s}(u), \tag{26}$$

in which $U_i^j = (\rho_i^j, q_i^j)$ is the average of $u(x,t)$ over ith cell at time $j\Delta t$, $\tilde{s}(u)$ is the average of the source term over $((i-1/2)\Delta x, (i+1/2)\Delta x) \times (j\Delta t, (j+1)\Delta t)$, and the boundary state $U_{i+1/2}^{*j} = (\rho_{i+1/2}^{*j}, q_{i+1/2}^{*j})$ is computed, as shown in the preceding subsection, from the Riemann problem for Equation 10 with initial condition

$$u_{i+1/2}(x, t_j) = \begin{cases} u_l, & \text{if } x - x_{i+1/2} < 0, \\ u_r, & \text{if } x - x_{i+1/2} \geq 0, \end{cases} \tag{27}$$

where $u_l = U_i^j$ and $u_r = U_{i+1}^j$.

Here, we use an implicit treatment of the source (relaxation) term and can write two finite difference equations for Equation 7,

$$\frac{\rho_i^{j+1} - \rho_i^j}{\Delta t} + \frac{\rho_{i+1/2}^{*j} v_{i+1/2}^{*j} - \rho_{i-1/2}^{*j} v_{i-1/2}^{*j}}{\Delta x} = 0,$$

$$\frac{v_i^{j+1} - v_i^j}{\Delta t} + \frac{\left[\frac{1}{2}(v_{i+1/2}^{*j})^2 - c_0 v_{i+1/2}^{*j}\right] - \left[\frac{1}{2}(v_{i-1/2}^{*j})^2 - c_0 v_{i-1/2}^{*j}\right]}{\Delta x} = \frac{V(\rho_i^{j+1}) - v_i^{j+1}}{\tau}.$$

From these two equations, we can find ρ and v at time step $j+1$ with given values at j.

4 THE FIFTH ORDER WEIGHTED ESSENTIALLY NON-OSCILLATORY METHOD

Since the Godunov method is based on solutions of the Riemann problem for the homogeneous system, Equation 10, it fails to have a solution when condition 25 is satisfied, especially when a vacuum problem occurs. However, as we know, the frozen-wave model is not homogeneous and has a relaxation term. Will this relaxation term make things better and help get rid of the occurrence of vacuum problems? I.e., is it possible that the frozen-wave model can still have physical solutions when condition 25 is satisfied? To help answer this question, we develop a fifth order WENO finite difference method (15) that does not require a Riemann problem solver. The advantage of this method is that the frozen-wave model can be solved even when condition 25 is satisfied since no Riemann solver is used. In this method, the 2×2 system of conservation laws, Equation 10, are first diagonalized into two independent,

single conservation laws, for each of which several groups of stencils are used to interpolate the variables and find their values at cell boundaries. Here the stencils are chosen based on "wind direction" (i.e. signs of the characteristic speeds $\lambda_{1,2}$) and weighted appropriately.

With the same partition and notations as in Subsection 3.3, we first compute $u_{i+1/2}$ and then $L(u_{i+1/2})$ $(i = 0, \cdots, N)$ in order to transform Equation 10 into Equation 11. To compute $u_{i+1/2}$, we use the simple arithmetic mean

$$\begin{bmatrix} \rho_{i+1/2} \\ v_{i+1/2} \end{bmatrix} = \begin{bmatrix} \frac{1}{2}(\rho_{i+1} + \rho_i) \\ \frac{1}{2}(v_{i+1} + v_i) \end{bmatrix}, \tag{28}$$

which also satisfies the mean value theorem

$$f(u_{i+1}) - f(u_i) = f'(u_{i+1/2})(u_{i+1} - u_i).$$

Hence we have $(i = 1, \cdots, N)$

$$\begin{bmatrix} v_i \\ w_i \end{bmatrix} = \begin{bmatrix} v_i \\ \rho_i + \frac{v_i}{c_0}\rho_{i+1/2} \end{bmatrix}. \tag{29}$$

Then we obtain a global conservation law for v

$$v_t + \left(\frac{1}{2}v^2 - c_0 v\right)_x = 0, \tag{30}$$

in which no parameters are determined by local cells, and a local conservation law for w:

$$w_t + \left(\rho v + \frac{\rho_{i+1/2}}{c_0}\left(\frac{1}{2}v^2 - c_0 v\right)\right)_x = 0, \tag{31}$$

in which there are parameters determined by local cells.

To solve the two equations with the WENO method, we denote $w_i = \rho_i + \frac{\rho_{i+1/2}}{c_0}v_i$, $g(v_i) = \frac{1}{2}v_i^2 - c_0 v_i$, and $h(w_i, v_i) = \rho_i v_i + \frac{\rho_{i+1/2}}{c_0}\left(\frac{1}{2}v_i^2 - c_0 v_i\right)$.

4.1 Boundary Flux of the Local Conservation Law

Since the local conservation law, Equation 31, has characteristic speed $v \geq 0$, we do not need to perform flux splitting. At jth time step, with given ρ_i, v_i, and w_i, we apply the fifth order WENO reconstruction procedure to find fluxes $h^{*j}_{i+1/2}$ as follows.

Introducing temporary variables $z_i = h(w_i, v_i)$ $(i = 1, \cdots, N)$, we apply the following process to obtain a fifth order WENO reconstruction of $h(w, v)$ to find $h^{*j}_{i+1/2} = z^-_{i+1/2}$:

$$\begin{aligned}
z^-_{i+1/2} &= \left(\alpha_0 z^{(0)}_{i+1/2} + \alpha_1 z^{(1)}_{i+1/2} + \alpha_2 z^{(2)}_{i+1/2}\right) / \left(\alpha_0 + \alpha_1 + \alpha_2\right), \\
z^{(0)}_{i+1/2} &= \frac{1}{3} z_i + \frac{5}{6} z_{i+1} - \frac{1}{6} z_{i+2}, \\
z^{(1)}_{i+1/2} &= -\frac{1}{6} z_{i-1} + \frac{5}{6} z_i + \frac{1}{3} z_{i+1}, \\
z^{(2)}_{i+1/2} &= \frac{1}{3} z_{i-2} - \frac{7}{6} z_{i-1} + \frac{11}{6} z_i, \\
\alpha_r &= \frac{d_r}{(\epsilon + \beta_r)^2}, \qquad r = 0, 1, 2,
\end{aligned}$$

where $\epsilon = 10^{-6}$, $d_0 = \frac{3}{10}$, $d_1 = \frac{3}{5}$, $d_2 = \frac{1}{10}$, and

$$\begin{aligned}
\beta_0 &= \frac{13}{12}(z_i - 2z_{i+1} + z_{i+2})^2 + \frac{1}{4}(3z_i - 4z_{i+1} + z_{i+2})^2, \\
\beta_1 &= \frac{13}{12}(z_{i-1} - 2z_i + z_{i+1})^2 + \frac{1}{4}(z_{i-1} - z_{i+1})^2, \\
\beta_2 &= \frac{13}{12}(z_{i-2} - 2z_{i-1} + z_i)^2 + \frac{1}{4}(z_{i-2} - 4z_{i-1} + 3z_i)^2.
\end{aligned}$$

4.2 Boundary Flux of the Global Conservation Law

For the global conservation law, Equation 30, whose characteristic speed $v - c_0$ can be positive or negative, we have to perform flux splitting. With flux splitting, we obtain an upwind flow (positive characteristic speed) and a downwind flow (negative characteristic speed), which can be interpolated independently and then combined

together. We define α as follows:

$$\alpha = \max_{1\le i\le N} |v_i - c_0|, \tag{32}$$

and then choose $g^{\pm}(v) = \frac{1}{2}(\frac{1}{2}v^2 - c_0 v \pm \alpha v)$ such that

$$\frac{\mathrm{d}g^+(v)}{\mathrm{d}v} \ge 0, \qquad \frac{\mathrm{d}g^-(v)}{\mathrm{d}v} \le 0.$$

Denoting $z_i = g^+(v_i)$ $(i = 1, \cdots, N)$, we can apply the same process as in the preceding subsection to find $z^-_{i+1/2}$.

Denoting $z_i = g^-(v_i)$ $(i = 1, \cdots, N)$, we can obtain a fifth order WENO reconstruction of $g^-(v)$ and find $z^+_{i-1/2}$ as follows:

$$\begin{aligned}
z^+_{i-1/2} &= \left(\alpha_0 z^{(0)}_{i-1/2} + \alpha_1 z^{(1)}_{i-1/2} + \alpha_2 z^{(2)}_{i-1/2}\right) / \left(\alpha_0 + \alpha_1 + \alpha_2\right), \\
z^{(0)}_{i-1/2} &= \frac{11}{6} z_i - \frac{7}{6} z_{i+1} + \frac{1}{3} z_{i+2}, \\
z^{(1)}_{i-1/2} &= \frac{1}{3} z_{i-1} + \frac{5}{6} z_i - \frac{1}{6} z_{i+1}, \\
z^{(2)}_{i-1/2} &= -\frac{1}{6} z_{i-2} + \frac{5}{6} z_{i-1} + \frac{1}{3} z_i, \\
\alpha_r &= \frac{d_r}{(\epsilon + \beta_r)^2}, \qquad r = 0, 1, 2,
\end{aligned}$$

where $\epsilon = 10^{-6}$, $d_0 = \frac{1}{10}$, $d_1 = \frac{3}{5}$, $d_2 = \frac{3}{10}$, and

$$\begin{aligned}
\beta_0 &= \frac{13}{12}(z_i - 2z_{i+1} + z_{i+2})^2 + \frac{1}{4}(3z_i - 4z_{i+1} + z_{i+2})^2, \\
\beta_1 &= \frac{13}{12}(z_{i-1} - 2z_i + z_{i+1})^2 + \frac{1}{4}(z_{i-1} - z_{i+1})^2, \\
\beta_2 &= \frac{13}{12}(z_{i-2} - 2z_{i-1} + z_i)^2 + \frac{1}{4}(z_{i-2} - 4z_{i-1} + 3z_i)^2.
\end{aligned}$$

Finally we have $g^{*j}_{i+1/2} = z^-_{i+1/2} + z^+_{i+1/2}$.

4.3 The Finite Difference Equations for the Frozen-Wave Model

Once we obtain the boundary fluxes $g^{*j}_{i+1/2}$ and $h^{*j}_{i+1/2}$, we can find the boundary fluxes for the original system as

$$f^{*j}_{i+1/2} = R\begin{bmatrix} g^{*j}_{i+1/2} \\ h^{*j}_{i+1/2} \end{bmatrix} = \begin{bmatrix} \bar{f}^{*j}_{i+1/2} \\ \tilde{f}^{*j}_{i+1/2} \end{bmatrix}, \tag{33}$$

where

$$\begin{aligned} \bar{f}^{*j}_{i+1/2} &= -\frac{\rho_{i+1/2}}{c_0} g^{*j}_{i+1/2} + h^{*j}_{i+1/2}, \\ \tilde{f}^{*j}_{i+1/2} &= g^{*j}_{i+1/2}. \end{aligned}$$

Then, with the optimal third order TVD Runge-Kutta method (15), we can update traffic conditions as follows. First, we compute the intermediate states $(\rho_i^{(1)}, v_i^{(1)})$:

$$\begin{aligned} \rho_i^{(1)} &= \rho_i^j + \Delta t \frac{\bar{f}^{*j}_{i-1/2} - \bar{f}^{*j}_{i+1/2}}{\Delta x}, \\ v_i^{(1)} &= v_i^j + \Delta t \left(\frac{\tilde{f}^{*j}_{i-1/2} - \tilde{f}^{*j}_{i+1/2}}{\Delta x} + \frac{V(\rho_i^j) - v_i^j}{\tau} \right). \end{aligned}$$

Then, with $(\rho_i^{(1)}, v_i^{(1)})$, we solve for the fluxes $\bar{f}^{*j}_{i+1/2}$ and $\tilde{f}^{*j}_{i+1/2}$ and obtain another group of intermediate states $(\rho_i^{(2)}, v_i^{(2)})$:

$$\begin{aligned} \rho_i^{(2)} &= \frac{3}{4}\rho_i^j + \frac{1}{4}\rho_i^{(1)} + \frac{1}{4}\Delta t \frac{\bar{f}^{*j}_{i-1/2} - \bar{f}^{*j}_{i+1/2}}{\Delta x}, \\ v_i^{(2)} &= \frac{3}{4}v_i^j + \frac{1}{4}v_i^{(1)} + \frac{1}{4}\Delta t \left(\frac{\tilde{f}^{*j}_{i-1/2} - \tilde{f}^{*j}_{i+1/2}}{\Delta x} + \frac{V(\rho_i^{(1)}) - v_i^{(1)}}{\tau} \right). \end{aligned}$$

Finally, with $(\rho_i^{(2)}, v_i^{(2)})$, we solve for the fluxes $\bar{f}^{*j}_{i+1/2}$ and $\tilde{f}^{*j}_{i+1/2}$ and obtain traffic conditions at $(j+1)$th time step:

$$\begin{aligned} \rho_i^{j+1} &= \frac{1}{3}\rho_i^j + \frac{2}{3}\rho_i^{(2)} + \frac{2}{3}\Delta t \frac{\bar{f}^{*j}_{i-1/2} - \bar{f}^{*j}_{i+1/2}}{\Delta x}, \\ v_i^{j+1} &= \frac{1}{3}v_i^j + \frac{2}{3}v_i^{(2)} + \frac{2}{3}\Delta t \left(\frac{\tilde{f}^{*j}_{i-1/2} - \tilde{f}^{*j}_{i+1/2}}{\Delta x} + \frac{V(\rho_i^{(2)}) - v_i^{(2)}}{\tau} \right). \end{aligned}$$

This concludes the WENO approximation of the frozen-wave model.

5 NUMERICAL SIMULATIONS OF THE FROZEN-WAVE MODEL

In this section, we perform numerical simulations using the frozen-wave model on a ring road. The model parameters are chosen as follows (21, 22): the unit length $l =$ 0.028 km, the relaxation time $\tau = 5$ s, the free flow speed $v_f = 5l/\tau$, the jam density $\rho_j = 180$ veh/km, and the sound speed $c_0 = 2.48445l/\tau$; the equilibrium speed-density relationship $V(\rho) = 5.0461[(1 + \exp\{[\rho/\rho_j - 0.25]/0.06\})^{-1} - 3.72 \times 10^{-6}]l/\tau$. Thus when $\rho_{c1} < \rho < \rho_{c2}$, condition 12 is violated and Equation 7 becomes unstable. Here the two critical densities, ρ_{c1} and ρ_{c2}, are solutions of $\lambda_* = \lambda_1$, i.e., $\rho V'(\rho) + c_0 = 0$.

The equilibrium functions $V(\rho)$ and $Q(\rho)$ are shown in Figure 2, in which the two critical densities are $\rho_{c1} = 0.173\rho_j$=31 veh/km and $\rho_{c2} = 0.396\rho_j$=71 veh/km.

The length of the ring road is $L = 800l$ and the time interval $[0, T]$, where $T = 500\tau$. In the numerical studies, we partition the roadway into N cells and the time interval into K steps, with $N/K = 1/10$; e.g., if $N = 100$ and $K = 1000$, the cell length is $\Delta x = 8l$ km and the length of each time step $\Delta t = 0.5\tau$ s. Since $\lambda_2 \leq v_f < 5l/\tau$, we find that the CFL (23) condition number $\lambda_2 \Delta t/\Delta x \leq 0.3125$.

With the Godunov method and the fifth order WENO method, we will show the simulation results of both stable and unstable traffic on the ring road.

5.1 Simulation of Stable Traffic

Here we use the following global perturbation as the initial traffic conditions:

$$\begin{aligned} \rho(x,0) &= \rho_h + \Delta\rho_0 \sin(2\pi x/L), \quad x \in [0,L], \\ v(x,0) &= V(\rho_h) + \Delta v_0 \sin(2\pi x/L), \quad x \in [0,L]. \end{aligned} \tag{34}$$

We set $\rho_h = 20$ veh/km, $\Delta\rho_0 = 3$ veh/km, and $\Delta v_0 = 0.002$ km/s. Then the initial conditions are inside the stable region of the frozen-wave model.

Setting $N = 100$ and $K = 1000$, we solve the frozen-wave model with both the Godunov method and the fifth order WENO method. We also solve the LWR model[4] and the PW model with the same conditions by using the Godunov method (5). The contour plots of ρ, v, and q are given in Figure 3, from which we can clearly see the formation of a forward traveling shock starting in the upstream half and a rarefaction wave starting in the downstream half of the road. Comparing the contour plots of ρ and q, we can see that flow rate starts to have the same evolution pattern as ρ after 100τ; i.e., after that, traffic conditions reach equilibrium and the frozen-wave model behaves nearly the same as the corresponding LWR model. Figure 4 compares the solutions of the LWR model, the PW model, and the frozen-wave model with the two methods. The figure shows that the frozen-wave model admits similar solutions as the LWR model and the PW model when it is stable. In this figure, that the solutions by the fifth order WENO method show sharper shocks than the other solutions is due to the very high accuracy of the method.

[4]Note that the initial travel speed for the LWR model, which is $v(x,0) = V(\rho(x,0)$, is different from that in Equation 34.

5.2 Simulation of Unstable Traffic

In this subsection, we still use initial conditions given in Equation 34, but with $\rho_h = 33$ veh/km. Thus the initial conditions are in the unstable region of the frozen-wave model.

When we partition the roadway into $N = 400$ cells, we find that the Godunov method fails in this case because condition 25 is satisfied and vacuum problems occur, but the fifth order WENO still works. In Figure 5, we illustrate solutions of the frozen-wave model by the fifth order WENO method and compare them to the solutions of the PW model. From this figure we can see that the frozen-wave model is capable of simulating spontaneous clusters for this partition, although the clusters in the frozen-wave model are much noisier than those in the PW model.

However, when we increase N to 1600; i.e., we partition the roadway into finer grids, the solutions of the frozen-wave model become unrealistic: as shown in Figure 6, the largest traffic density is higher than the jam density ρ_j. These non-physical solutions are believed to be related to condition 25. [5] In addition, densities go much bigger than the jam density and will eventually blow up when we further increase the number of cells in the simulation. Since numerical solutions are heavily dependent on the number of cells, the solutions are unreliable. Therefore, it suggests that the frozen-wave model does not have reasonable solutions under the given initial conditions. We believe that this phenomenon is un-avoidable due to the occurrence of vacuum problems.

[5] We have also tried to extend the fundamental diagram by 0 for densities greater than the jam density, but still obtain non-physical solutions.

6 CONCLUSIONS

In this paper, an anisotropic nonequilibrium model, the frozen-wave model given by Equation 7, is studied. Our analysis show that this model has serious limitations because, when condition 25 is satisfied, the Riemann problem of Equation 10 is ill-posed in the sense that it admits non-physical solutions (with densities larger than the jam density) or vacuum problems occur (no solutions). From numerical simulations, we found that the model behaves similarly to the LWR and PW models when it is stable. However, when traffic is unstable, both the Godunov and the fifth order WENO numerical solution methods fail to produce physical solutions. Hence, both analytical and numerical studies indicate that the frozen-wave model has serious limitations and that this model can not simulate the formation of vehicle clusters as the PW model does (6).

The studies here suggest that it is premature to consider the frozen-wave model as an alternative to the LWR and PW models. This does not imply, however, that other members in the ARZ model class cannot. We suspect the problems of the frozen-wave model derive from its adoption of a constant "sound" wave speed c_0. Our further work will explore alternative "sound" wave specifications in the ARZ model class and study their solution properties as compared to the LWR and PW models.

In addition to the findings on the properties of the frozen-wave model itself, the numerical methods developed here, especially the fifth order WENO method, can be applied in solving other continuum traffic flow models.

References

[1] M. J. Lighthill and G. B. Whitham. On kinematic waves: II. a theory of traffic flow on long crowded roads. *Proceedings of the Royal Society of London A*, 229: 317–345, 1955.

[2] P. I. Richards. Shock waves on the highway. *Operations Research*, 4:42–51, 1956.

[3] H. J. Payne. Models of freeway traffic and control. In *Mathematical Models of Public Systems*, volume 1 of *Simulation Councils Proceeding Series*, pages 51–60, 1971.

[4] G. B. Whitham. *Linear and nonlinear waves*. John Wiley and Sons, New York, 1974.

[5] W. L. Jin and H. Michael Zhang. Solving the Payne-Whitham traffic flow model as a hyperbolic system of conservation laws with relaxation. 2001. In draft.

[6] W. L. Jin and H. Michael Zhang. The formation and structure of vehicle clusters in the payne-whitham traffic flow model. *Transportation Research B*, 2001. In press.

[7] Carlos F. Daganzo. Requiem for second-order fluid approximations of traffic flow. *Transportation Research B*, 29(4):277–286, 1995.

[8] A. Aw and M. Rascle. Resurrection of "second order" models of traffic flow. *SIAM Journal on Applied Mathematics*, 60(3):916–938, 2000.

[9] H. Michael Zhang. A theory of nonequilibrium traffic flow. *Transportation Research B*, 32(7):485–498, 1998.

[10] H. Michael Zhang. A non-equilibrium traffic model devoid of gas-like behavior. *Transportation Research B*, 36(3):275–290, 2002.

[11] Tong Li. Global solutions of nonconcave hyperbolic conservation laws with relaxation arising from traffic flow. *Journal of Differential Equations*, 2001. Submitted.

[12] H. Michael Zhang. Some extensions to an anisotropic nonequilibrium traffic flow model, 2000. Unpublished manuscript.

[13] R. Jiang, Q.-S. Wu, and Z.-J. Zhu. A new continuum model for traffic flow and numerical tests. *Transportation Research B*, 36:405–419, 2002.

[14] S. K. Godunov. A difference method for numerical calculations of discontinuous solutions of the equations of hydrodynamics. *Matematicheskii Sbornik*, 47:271–306, 1959. In Russian.

[15] C. W. Shu. Essentially non-oscillatory and weighted essentially non-oscillatory schemes for hyperbolic conservation laws. In B. Cockburn, C. Johnson, C. W. Shu, E. Tadmor, and A. Quarteroni, editors, *Advanced Numerical Approximation of Nonlinear Hyperbolic Equations*, volume 1697 of *Lecture Notes in Mathematics*, pages 325–432. Springer, New York, 1998.

[16] G. B. Whitham. Some comments on wave propagation and shock wave structure with application to magnetohydronamics. *Communications on Pure and Applied Analysis*, XII:113–158, 1959.

[17] T. P. Liu. Hyperbolic conservation laws with relaxation. *Communications in Mathematical Physics*, 108:153–175, 1987.

[18] G. Q. Chen, C. D. Levermore, and T. P. Liu. Hyperbolic conservation laws with stiff relaxation terms and entropy. *Communications on Pure and Applied Mathematics*, XLVII:787–830, 1994.

[19] J. Smoller. *Shock waves and reaction-diffusion equations*. Springer-Verlag, New York, 1983.

[20] P. D. Lax. *Hyperbolic systems of conservation laws and the mathematical theory of shock waves*. SIAM, Philadelphia, Pennsylvania, 1972.

[21] Boris S. Kerner and P. Konhäuser. Structure and parameters of clusters in traffic flow. *Physical Review E*, 50(1):54–83, 1994.

[22] M. Herrmann and Boris S. Kerner. Local cluster effect in different traffic flow models. *Physica A*, 255:163–198, 1998.

[23] R. Courant, K. Friedrichs, and H. Lewy. ber die partiellen differenzengleichungen der mathematischen physik. *Mathematische Annalen*, 100:32–74, 1928.

List of Figures

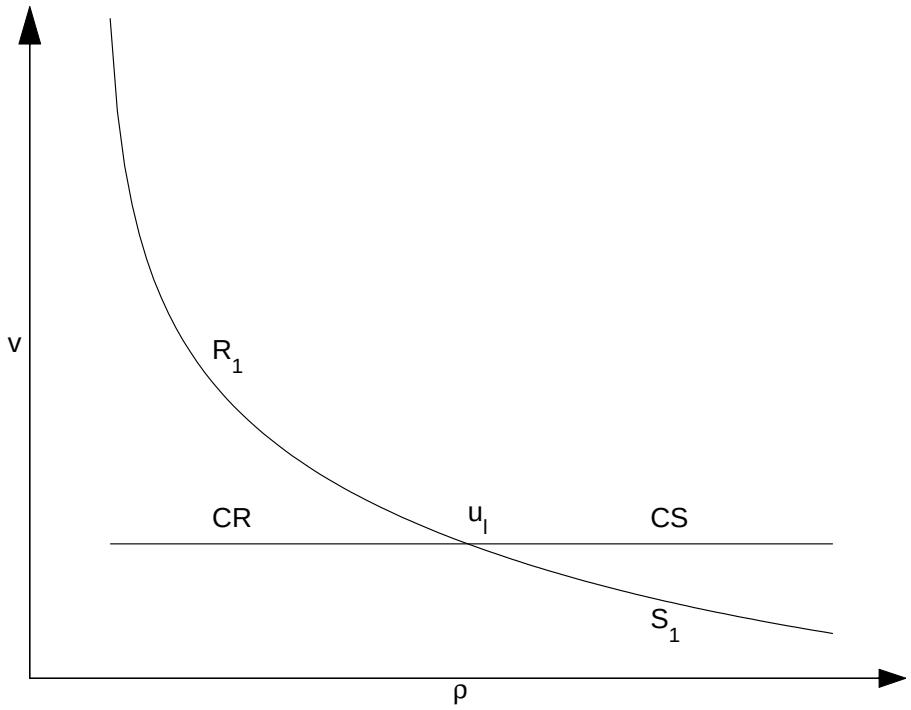

Figure 1: **Basic Curves in the (ρ, v)-Plane**

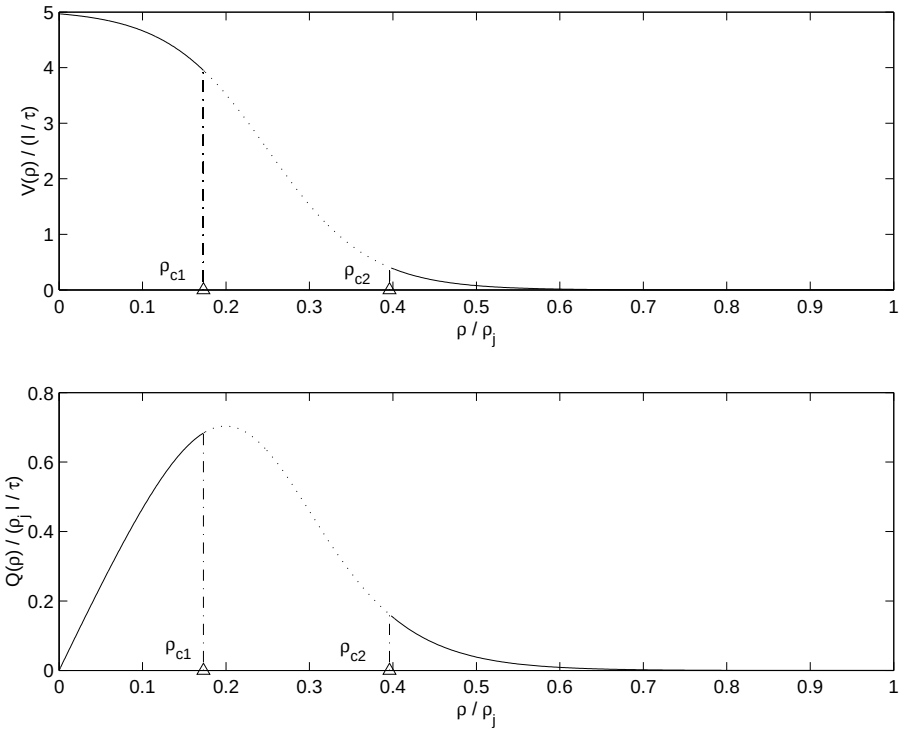

Figure 2: **The Kerner-Konhäuser (1994) Model of Speed- and Flow-Density Relations**

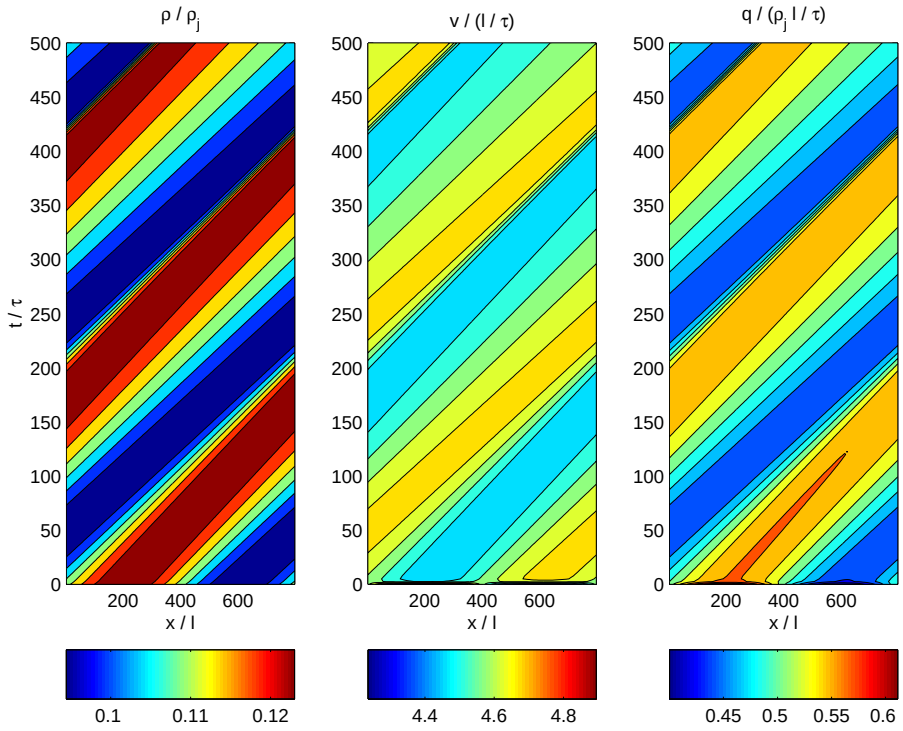

Figure 3: **Contour Plots of Stable Solutions of the Frozen-Wave Model by the Fifth Order WENO Method: A Forward Traveling Shock Starts in the Upstream Half Road and a Rarefaction Wave Starts in the Downstream Half Road. After 100τ, Traffic Conditions Reach Equilibrium and the Frozen-Wave Model Behaves Almost the Same as the Corresponding LWR Model**

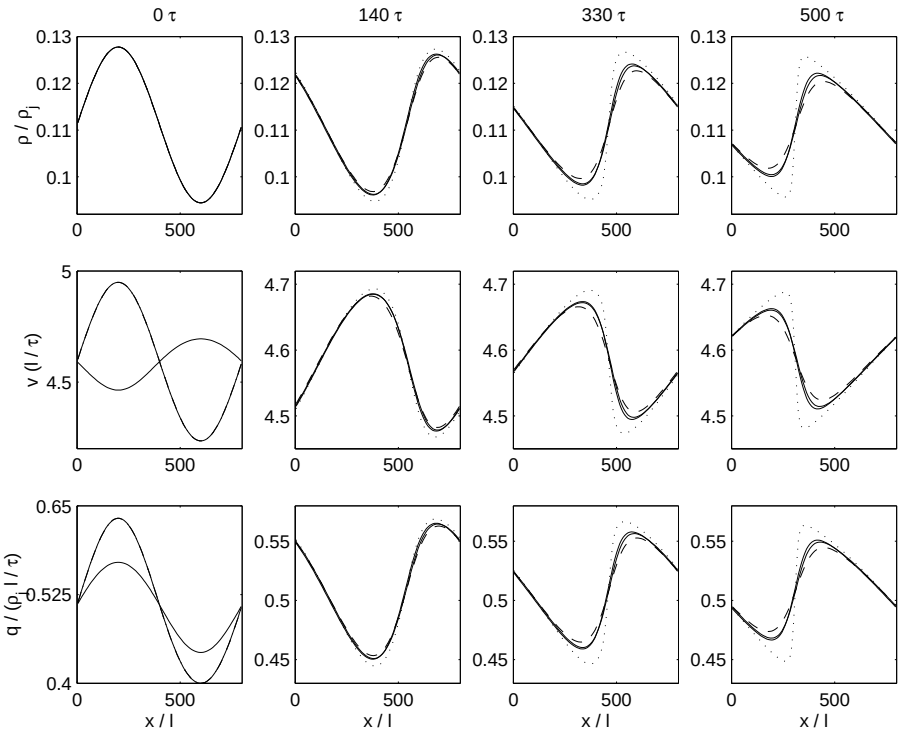

Figure 4: **Comparison of Solutions of the LWR, PW, and Frozen-Wave Models on a Homogeneous Roadway: Thinner Solid Lines for the LWR Model, Dashed Lines for the PW Model, Thicker Lines for the Frozen-Wave Model with the Godunov Method, and Dotted Lines for the Frozen-Wave Model with the Fifth Order WENO Method**

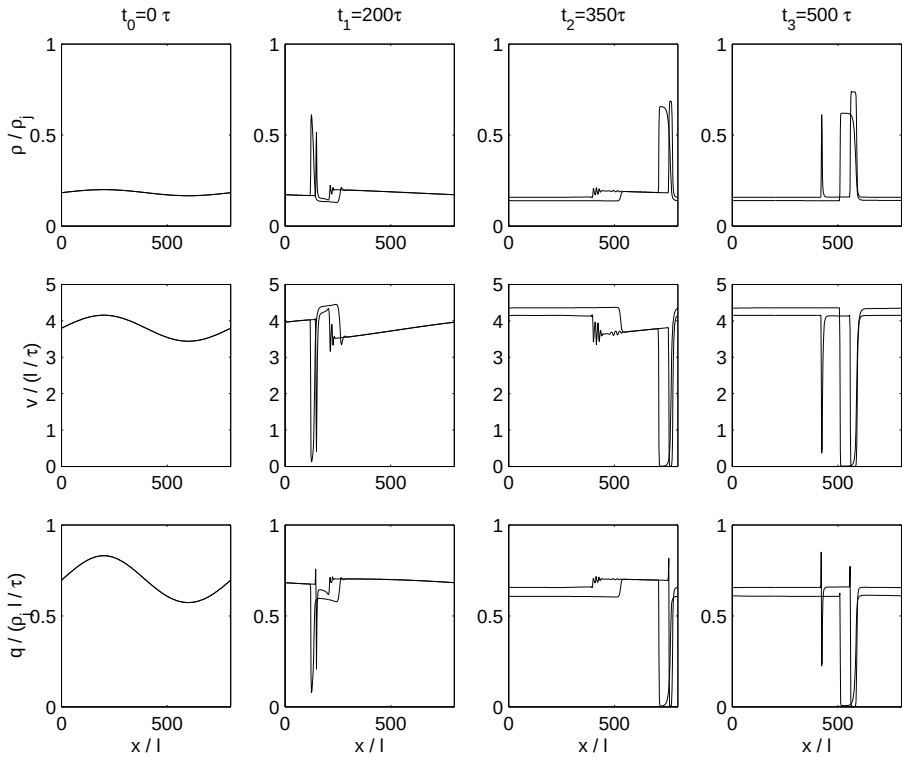

Figure 5: **Cluster Solutions of the Frozen-Wave Model and the PW Model When $N = 400$ at 0τ, 200τ, 350τ, and 500τ: Thinner Lines for the PW Model and Thicker Lines for the Frozen-Wave Model with the Fifth Order WENO Method**

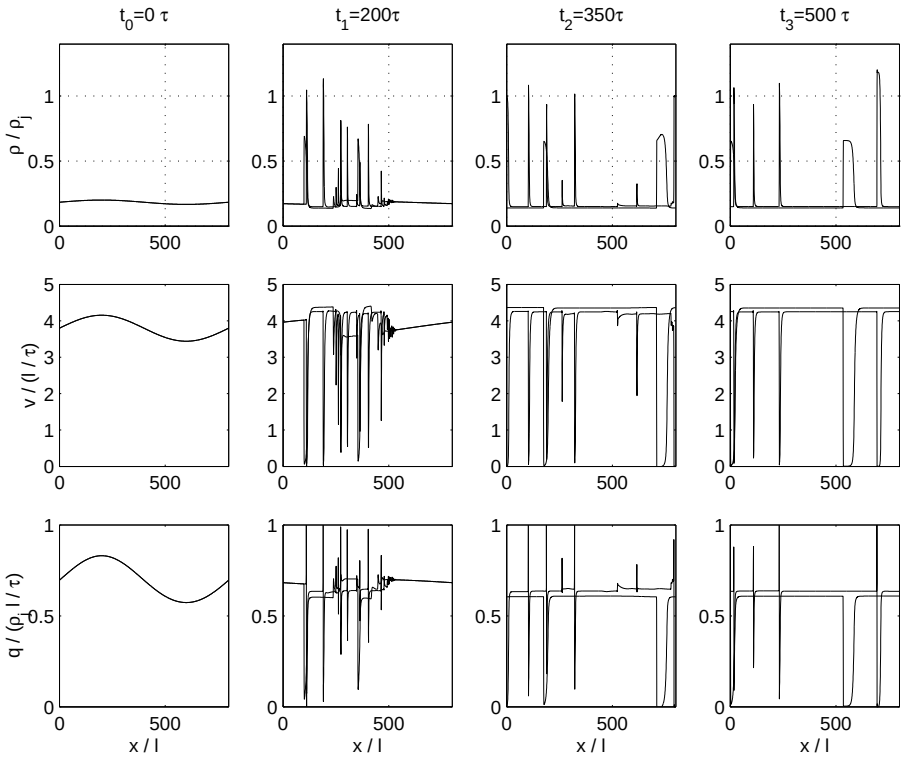

Figure 6: **Cluster Solutions of the Frozen-Wave Model and the PW Model When $N = 1600$ at 0τ, 200τ, 350τ, and 500τ: Thinner Lines for the PW Model and Thicker Lines for the Frozen-Wave Model with the Fifth Order WENO Method**